Journal of
Materials Chemistry C

Materials for optical, magnetic and electronic devices

Accepted Manuscript

This article can be cited before page numbers have been issued, to do this please use: J. bi, H. wu, Z. zhang, A. Zhang, H. Yang, Y. feng, F. yi, L. zhang, Z. wang, W. qu, F. Liu and C. Zhang, *J. Mater. Chem. C*, 2019, DOI: 10.1039/C9TC04349G.

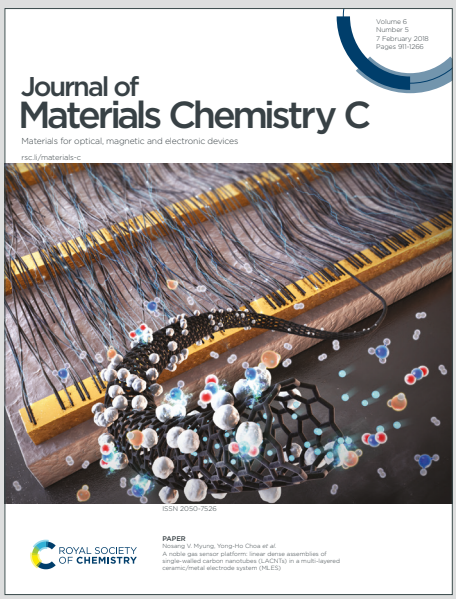

ROYAL SOCIETY OF CHEMISTRY

rsc.li/materials-c

View Article Online
DOI: 10.1039/C9TC04349G

ARTICLE

Highly Ordered Columnar Superlattice Nanostructures with Improved Charge Carrier Mobility by Thermotropic Self-assembly of Tripheylene-based Discotics

Received 00th January 20xx,
Accepted 00th January 20xx

DOI: 10.1039/x0xx00000x

Jingze Bi[a], Hao Wu[a], Zhenhu Zhang[a], Ao Zhang[a], Huanzhi Yang[a], Yuwen Feng[a], Yi Fang[a], Lina Zhang[a], Zhengran Wang[a], Wentao Qu[b], Feng Liu[*b], Chunxiu Zhang[*a]

A series of triphenylene esters with two ester groups at 2,3-, 2,7-, 2,6- and 3,6- substituent positions was successfully synthesized and fully investigated. Their self-assembly properties were exhaustively examined by DSC, POM, 1DXRD, 2DXRD, SAXS, TEM methods together with EDM, ESP calculations. It was unexpected that 3,6-substituted triphenylene ester T5E36 formed an uncommonly helical hexagonal columnar superlattice structure made up of 9_1 right-handed helixes with a pitch of 60.3Å. This helical superlattice structure was further studied by transmission electron microscopy the diameter of T5E36 particles was found to be at nanometer scale. Ultimately, the bipolar charge carrier mobility was measured by time-of-flight method at the order up to 10^{-1} $cm^2V^{-1}s^{-1}$. The formation of this helical superlattice nanostructure no doubt improved their electronic properties and made them more attractive in organic electronics.

Introduction

To construct highly ordered molecular stacking structures as well as nanostructures with sophisticated optoelectronic properties by the assembly of discotic molecules is always an ultimate goal of researchers in the field of discotic liquid crystals (DLCs). DLCs are expected to be excellent charge carrier transport materials in optoelectronics devices such as field effect transistors, photovoltaic solar cells and light emitting diodes [1-6]. Recent studies on ester groups substituted triphenylene DLCs have demonstrated that the dipole-dipole interactions of polar groups have a special guidance on the order and scale of self-assembled mesophase structures.

The first triphenylene based DLCs, hexa-n-alkanotes triphenylenes, which were symmetrical hexasubstituted triphenylene esters were recognized by Billard, Dubois and Destrade in 1979 after the discovery that disc-shaped molecules benzene-hexa-n-alkanoates could form liquid crystals of Chandrasekhar in 1977 [7-9]. Early studies of triphenylene esters mainly focused on the new symmetrical hexasubstituted and asymmetrical mono-, di- and tri-substituted compounds. Interestingly, they exhibited the characteristic hexagonal columnar (Col_h) phases that were found to be monotropic mesophases [10-12]. Compared with triphenylene ethers which were the counterparts of another big part of DLCs, mesogenic triphenylene ester derivatives showed decreases in the melting point and substantial broadenings in the liquid crystal phases. That was, the Col_h phase can be maintained even at room temperature and this ordered structure can be suppressed in glassy states [13-15]. Spiess and coworkers reported an unsymmetrical chiral ester groups substituted pentakis(pentyloxy)triphenylene and proposed that the steric effects strongly stabilized the intramolecular interactions due to the preferred out-of-plane conformations and the dipole moments of ester substituents. These intramolecular interactions significantly increased the clearing temperatures and suppressed the crystallizations giving rise to substantially lower glass transition temperatures

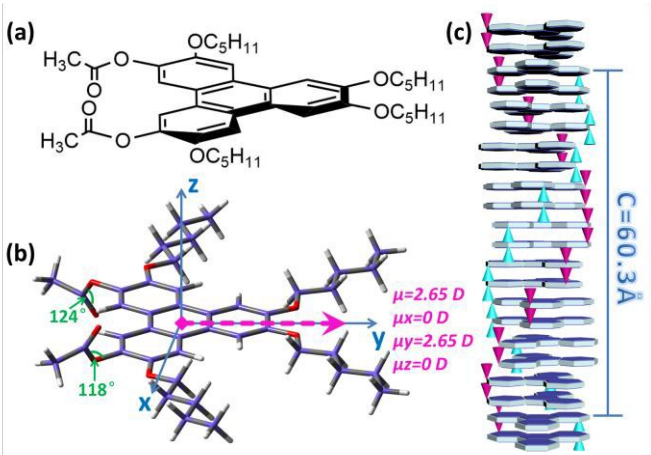

Fig. 1 a) Molecular formula of T5E36; b) Optimized conformation and dipole moment of T5E36; c) Helical column of T5E36.

[a] Information Recording Materials Lab, Beijing Key Laboratory of Printing & Packaging Materials and Technology, Beijing Institute of Graphic Communication, Beijing, 102600 (P. R. China), E-mail: zhangchunxiu@bigc.edu.cn
[b] State Key Laboratory for Mechanical Behaviour of Materials, Shaanxi International Research Center for Soft Matter, Xi'an Jiaotong University, Xi'an 710049 (P. R. China), E-mail: feng.liu@xjtu.edu.cn

Electronic Supplementary Information (ESI) available: See DOI: 10.1039/x0xx00000x

[16]. Their another work reported a superstructure existed in the chiral ester group substituted pentakis(pentyloxy)triphenylene for the occurrence of an additional peak at small angle region. However, the insight of this superstructure could not be fully elucidated at that time [17]. Simultaneously, Wendorff and coworkers synthesized another type of mono-substituted triphenylene carboxylic esters based on hexapentyloxytriphenylenes (HAT5). The reflection near 2ϑ = 2.5° in the small angle region of XRD pattern was the first evidence for the formation of a novel discotic mesophases superstructure caused by bulky substituents and polar substituents [18].Takuzo Aida and coworkers restudied the mesophases of triphenylene hexacarboxylic esters and confirmed that even a small aromatic mesogen such as triphenylene esters enabled an exceptionally wide-range 2D lattice correlation owing to the intercolumnar dipole–dipole interaction which lead to a large-area homeotropic columnar orientation. A rather high hole mobility was obtained along with its anisotropic nature up to $5x10^{-3}$ $cm^2V^{-1}s^{-1}$ [19]. Takanori Fukushima and coworkers constructed a novel dibenzo[a,c]phenazine disc-molecule with a large dipole moment. The synchrotron radiation XRD results confirmed the formation of a 2D superlattice structure via the hierarchical columnar assemblies of discotic liquid crystals [20]. Our recent works based on triphenylene esters also exhibited the supperlattice nanostructures with high charge carrier mobility [21-23]. Nevertheless, how the substituted positions decisively influenced the properties of the molecules not only in complanate two dimensional lattice correlations but also in three dimensional lattice structures was still unsolved.

Experimental section

Materials

All chemicals were purchased from Aladdin, and all solvents from Aldrich. All chemicals and solvents were used without further purification. Silica gel 60 (200-300 mesh ASTM) and silica gel 60 glass thin-layer chromatography were used for the purification and identification of the reactions, respectively.

Instrumentations

The ^{1}H-NMR spectra were recorded by a Bruker NMR spectrometer (DMX 300 MHz) in $CDCl_3$, Chemical shifts are given as units of measurement and expressed in parts per million (δ) with tetra-methylsilane (TMS) as a reference. Multiplicities of peaks are expressed as s = singlet, d = doublet, t = triplet, m = multiplet; The KBr pellets were used to make the test samples and the infrared spectrum (FT-IR) was recorded on a Shimadzu FTIR-8400 spectrometer by Fourier transform; The high resolution mass spectrum was recorded on a Bruker Apex IV FTMS mass spectrometer. Elemental analysis (C, H) was performed on an Elementar Vario EL CUBE elements analyzer. The thermal properties of discotic liquid crystals were characterized by using differential scanning calorimeter (DSC) on a Netzsch DSC 200. Its optical properties were characterized by a Polarizing Microscope (POM) on a Leica DM4500P with a Linkam TMS94 hot stage. The structural characterizations of samples were characterized by 1D X-ray diffraction (1DXRD) through a Bruker D8 Advance diffractometer equipped with a variable temperature controller; two-dimensional X-ray diffraction (2DXRD) using a 40KV FL tube as the X-ray source (Cu Ka) and the small-angle X-ray scattering (SAXS) (SAXSess, Anton Paar) equipped with Kratky block-collimation system. The structure and morphology were investigated by Transmission Electron Microscope (FEI Tecnai G2 20 STWIN).

Syntheses

As the workhorse of discotic liquid crystals, triphenylenes have been frequently studied since they are relatively easy to be synthesized and processed. The syntheses of intermediates functional di-hydroxyl substituted triphenylenes were based on previous works. For 2,3-di-hydroxyl-6,7,10,11-tetrapentyloxytriphenylene, the synthetic route by using lithium diphenylphosphine as a catalyst to make cleavage of two methyloxyl groups reported by Bushby in the year of 1995 [24]. The 2,7-di-hydroxyl-3,6,10,11-tetrapentyloxytriphenylene was hard to be synthesized, but we are still enable to employ the general regiospecific synthesis reported by Boden in 1995 which was very similar to the synthesis of 2,3-di-hydroxyl-6,7,10,11-tetrapentyloxytriphenylene [25]. For 2,6-di-hydroxyl-3,7,10,11-tetrapentyloxytriphenylene, we used a synthetic procedure for the preparation of di- and tri- functional triphenylene derivatives starting from the readily available hexakis(pentyloxy)triphenylene by selective ether cleavages with B-bromocate-cholborane reported by Kumar in 1997, which mainly obtained 2,6-, 2,6,10- and 2,7,11- hydroxyl substituted triphenylene derivatives [13]. For 3,6-di-hydroxyl-2,7,10,11-tetrapentyloxytriphenylene, we took a click-on method reported by our group in 2014 with very high yield up to 24.7% [26]. The detailed syntheses of T5E23, T5E27, T5E26 and T5E36 are provided in ESI.

Results and discussion

Herein, we successfully synthesized triphenylene esters T5E23, T5E27, T5E26 and T5E36 with two ester groups at different substituent positions where T, 5 and E refer to triphenylene, pentyloxy and ethoxycarbonyl, respectively, while 23, 27, 26 and 36 refer to the substituent positions of ethoxycarbonyl. Their mesophases and self-assembly properties have been systematically studied and shown in Fig.2.

Considering the results of the polarizing optical microscopy (POM), differential scanning calorimetry (DSC) and one-dimensional X-ray diffraction (1DXRD) **(Fig. 2, S9, S10)**, T5E23 and T5E27 showed hexagonal columnar phases during the cooling. But ultimately their crystallizations at room temperature broke the liquidity, continuity and peculiar physical property of liquid crystals, which were not conducive to their applications.T5E26 and T5E36 showed pseudo focal conic textures that have been proved to be typical hexagonal columnar textures at 160°C and 165°C during the cooling, respectively, which can be maintained at the room temperature without any changes in liquid crystal textures [27]. The DSC results of T5E26 showed only an exothermic peak at 168.1°C during heating and an endothermic peak at 164.2°C during cooling. Nevertheless, T5E36 showed two exothermic peaks at 134.9°C and 173.1°C during heating as well as two endothermic peaks at 121.1°C and 167.4°C during cooling. Combining with the 1DXRD data of T5E36 obtained at 30°C, 100°C and 150°C during second heating **(Fig. 2d)**, the diffraction peaks in the range of 2ϑ = 5~20° can be indexed to (100), (110), (200) and (210) with the reciprocal *d*-spacing ratios 1,1/√3,1/2,1/√7 which were attributed to hexagonal packing [28]. When the temperature dropped to 30°C, under the second phase transition temperature of T5E36, the sharp diffraction peak in the wide angle region (about 2ϑ = 26°) split into two peaks, which was the evidence of a more ordered hexagonal columnar phase.

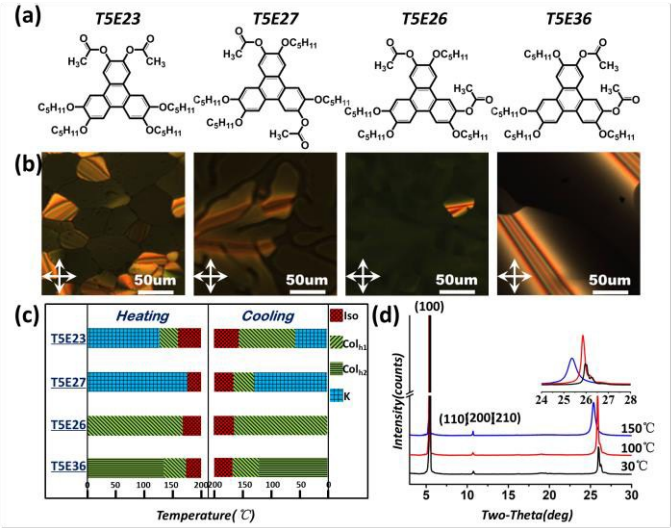

Fig. 2 a) Molecular formulas of T5E23, T5E27, T5E26 and T5E36 (from left to right); b) POM images of T5E23 at 135°C, T5E27 at 155°C, T5E26 at 160°C and T5E36 at 165°C (from left to right) with scale bar = 50μm; c) Graph of phase transition temperatures on heating (left column) and cooling (right column) based on the 1st cooling process and 2nd heating process by DSC(Iso=isotropic phase, Col_h=hexagonal columnar phase and K = crystalline phase); d) 1DXRD patterns of T5E36 at 30°C, 100°C and 150°C.

The 1DXRD patterns, lacked of lattice dimensionality of the liquid crystalline structure, were not adequate to analysis more detailed structures. So we collected two-dimensional X-ray diffraction (2DXRD) and small-angle X-ray scattering (SAXS) patterns of T5E26 and T5E36 **(Fig. 3a, b)**. After careful purification of the samples, we put the purified samples into a cuboid container made of aluminum foil, ensuring the thickness was about 10 μm. Whereafter, the samples were

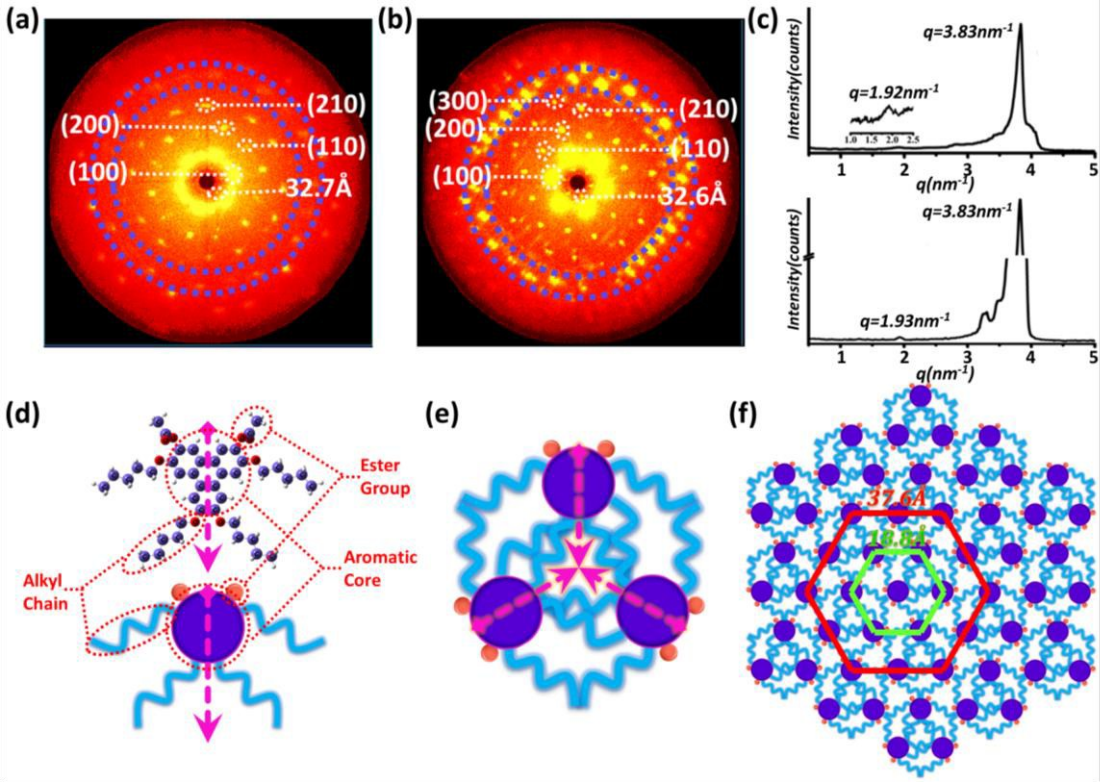

Fig. 3. 2DXRD patterns of oriented samples at room temperature: a) T5E26; b) T5E36; c) SAXS diffractograms of T5E26 (up) and T5E36 (down) recorded at room temperature; d) Optimized conformation and schematic diagram of T5E36 (pink arrow: the direction of dipole moment); e) Self-assembly of three T5E36 molecules; f) Model of hexagonal lattice and hexagonal superlattice.

placed on a heating stage and annealed from the temperature just below clearing point to room temperature over a whole night at a rate of 0.5°C/min. Eventually, good samples with monodomains for 2D WAXD measurement were obtained. Both T5E26 and T5E36 presented ordered diffraction spots in the low angle region that can be designated as (100), (110) (200) and (210), respectively, indicating that incident beam was perpendicular to the molecular plane [29]. Nevertheless, there were also six distinct diffraction spots corresponding to another 100 plane appeared in the inner region with the d-spacings equaled to 32.7Å and 32.6Å of T5E26 and T5E36, respectively. In combination with the results of SAXS patterns **(Fig. 3c)**, it was confirmed that the *d*-spacings of the inner region was almost twice as the *d*-spacings of (100) in hexagonal lattice which was 16.4Å and 16.3Å for T5E26 and T5E36, respectively. According to our previous works on 2D superlattice nanostructures, it was confirmed that T5E26 and T5E36 formed 2D superlattice under the guidance of long-range dipole-dipole interactions. The *a* parameters were calculated to be a_{colh1} = 18.9Å, a_{colh2} =37.8Å for T5E26 and a_{colh1} = 18.8Å, a_{colh2} = 37.6Å for T5E36 in hexagonal lattice and hexagonal supperlattice respectively [30]. For T5E36, each molecule only possessed a large dipole moment in plane from center of two ester groups to opposite alkyl chains showed as pink arrow **(Fig. 3d)** which must be cancelled out in order to get the steadiest and the most compact stacking. With flexible alkyl chains located in the center, three molecules assembled into a triangular shaped building block from three directions to minimize the net dipole and the contact area of side chains **(Fig. 3e)**. This triangular shaped building block was essential for the formation of hexagonal closest packing and arranged latterally to form an extented hexagonal lattice **(Fig. 3f)**.

Different from T5E26, 2DXRD pattern of T5E36 showed a series of sharp diffractions of high intensity in wide angle region (2ϑ = 19°±1°, *d* = 4.6±0.1Å) marked with purple circles **(Fig. 3a, b)**. In order to get the insight of the structure of T5E36,

View Article Online
DOI: 10.1039/C9TC04496

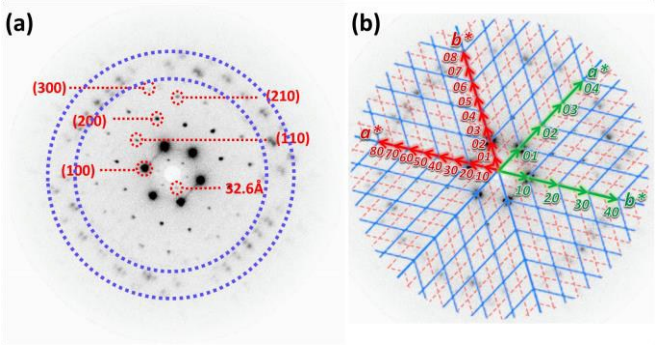

Fig. 4. a) Linearly adjusted 2DXRD pattern of T5E36; b) Reciprocal lattice of T5E36 (green arrows and blue lines: hexagonal lattice, red arrows and orange line: hexagonal superlattice).

subsequently, we linearly adjusted the intensity **(Fig. 4a)** and reconstructed the reciprocal lattice space **(Fig. 4b)** of T5E36 pattern. Superficially, these diffraction spots always came in pairs and some of these diffractions did not belong to both of the two hexagonal lattices exhibiting a higher intensity. The powder 2DXRD pattern of T5E36 **(Fig. S12)** also performed an obvious diffraction halo when *d*-spaceing was near 4.6Å, which was stronger than other diffractions except for (100) and π-π stackings. These results evidenced the ordered arrangement of the peripheral ester groups and further implied the existence of a more ordered hexagonal phase.

In order to expound further on the phase structure of T5E36, we prepared the oriented sample by mechanical shearing with a mild external force at 120°C just below the isotropic temperature, followed by fast cooling to room temperature. After that, sheared T5E36 sample was placed vertically on the sample stage to make sure that the incident

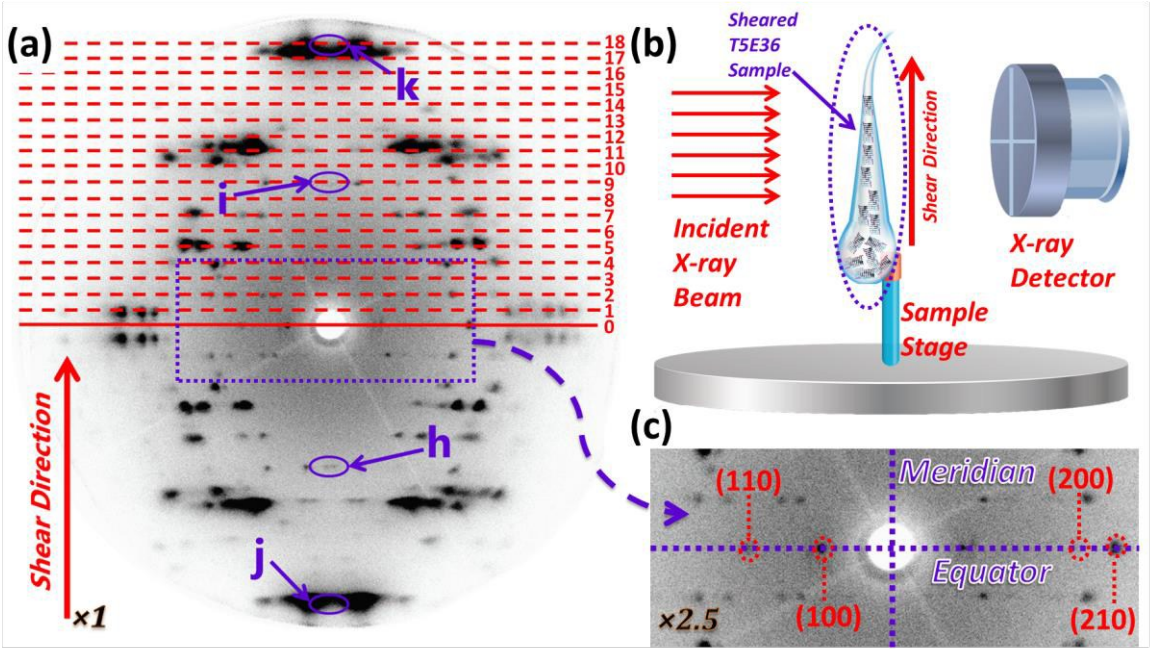

Fig. 5. a) 2DXRD patterns of sheared T5E36 at room temperature with shear direction and layer lines labelled; b) Schematic diagram of 2DXRD measurement of sheared T5E36 sample; c) Enlargement in low angle region with meridian and equator labelled.

X-ray beam can be perpendicular to shear direction **(Fig. 5b)**. **Fig. 5a** showed the 2DXRD pattern of sheared sample which was recorded at room temperature. The (*hk*0) diffractions of the hexagonal phase at low angle region on the equator **(Fig. 5c)** can be designated as (100), (110), (200) and (210) indicating that the axes of columns were well aligned along the shear direction (the meridian). The numerous sharp meridional and off-meridional diffractions demonstrated a periodic organization of molecules along the columns with long range intra- and intercolumnar order. Furthermore, the cross-like pattern of diffractions and 18 overt layer lines can be inferred to a helical arrangement in the columns [31-33]. The first diffractions on the meridian (i and h) which was corresponded to the subunit axial translations *H* appearing at 6.7Å was attributed to layer line *L* = 9. Thus, a helical pitch and repeat containing 9 subunits can be well defined. This kind of self-assembly structure was classified as a 9_1 helix with a pitch of *P* = 6.7Å×9 = 60.3Å which was also corresponded to reciprocal distance between equator and layer line *L* = 1 [34,35]. In the meantime, the strong diffractions emerged on the meridian at 3.4Å (k and j) which was attributed to layer line *L* = 18 in the wide angle region represented a compact π-π stacking between adjacent molecules. So the lattice parameters for T5E36 were calculated to be *a* = *b* = 18.8Å, *c* = 60.3Å and *γ* = 120°.

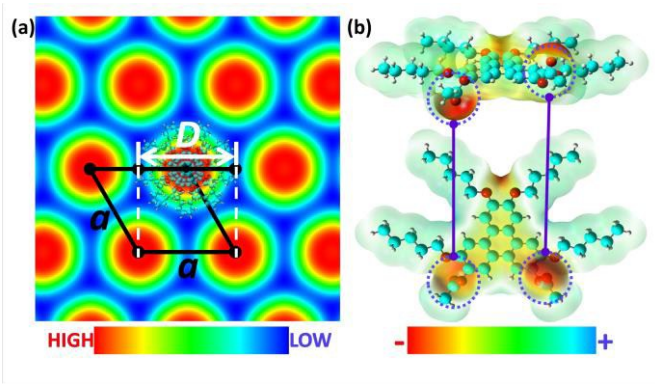

Fig. 6. a) Reconstructed electron density map of T5E36 with scale bar from high density (red) to low density (blue); b) Electrostatic potential isosurface calculations of T5E36 with scale bar from negative electrostatic potential (red) to positive electrostatic potential (light blue).

To investigate the model of T5E36 deeply, the electron density map (EDM) reconstructed from 1DXRD data at 30°C and the electrostatic potential (ESP) isosurface calculations at the B3LYP/6-31+G(d,p)//B3LYP/6-31G(d) level with Gaussian 09 package (Revision C.01) were performed **(Fig. 6)** [35-37]. Each red area with the highest electron density represented positions of the aromatic core of the triphenylene, while the surrounding yellow, green and blue areas were packed with ester groups and alkyl tails. As the *a* parameter of hexagonal lattice labeled in **Fig. 6a**, the white arrow line that was the diameter of columns equaled to the distance between adjacent columns and also equaled to the *a* parameter of the hexagonal lattice. Therefore, the diameter of each column in this hexagonal lattice D_{column} equaled to 18.8Å. In **Fig. 6b**, the 3,6 position ester groups of T5E36 out of the triphenylene plane in contradictory directions possessed a high value of electrostatic potential. This electrostatic potential gave the opportunity to an ordered arrangement of the peripheral ester groups which were already observed from 2DXRD pattern of T5E36.

With the help of all the results above, we reconstructed the model of molecules and supramolecular columns **(Fig. 7)**. As so many alkyl chains were not good for clarity, we only used polyhedrons and circular cones to represent triphenylene cores and ester groups respectively. The subunit axial translations *H* = 6.7Å which was twice the distance of adjacent molecules indicated that two T5E36 molecules rotated together with the azimuthal rotation angle *φ* = 360/9 = 40°. This angle also led to a constant distance between intramolecular ester groups out of plane in contradictory direction, which was about 4.6Å and can be easily observed in the 2DXRD pattern because of the intense electronic interaction of ester groups. As the T5E36 only had a C_2 symmetry axis in plane, two different rotations of the molecules can lead to right-handed and left-handed helixes. However, the distance between adjacent ester groups of left-handed helix was much larger than 4.6Å which will also reduce the molecules stability decisively. In order to accomplish a more stable and compact conformation, T5E36 tended to form right-handed helical columns. These columns also possessed a large *c* parameter of 60.3Å which was formed due to the triphenylene core and ester groups seeking the opportunity of close packing simultaneously. The most possible manner was

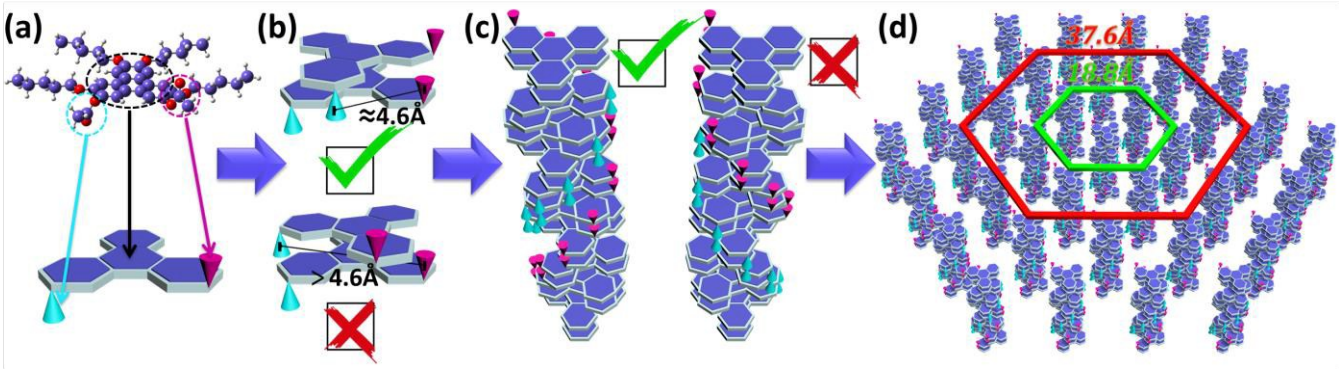

Fig. 7. Possible models of T5E36 with green ticks refer to right arrangement and red crosses refer to wrong arrangement: a) Model of triphenylene core; b) Result of two different rotations; c) Right-handed helix (left) and left-handed helix (right); d) Model of supramolecular columns.

just a slight rotation of molecules with respect to others in the column and helically assembled along the column axis, forming a 9-fold helix.

This long-range superlattice nanostructure can be easily perceived in transmission electron microscopy (TEM) which was considered to be an essential way to characterize the morphology of self-assembly structures. **Fig. 8** showed the TEM (FEI Tecnai G2 20 STWIN) image of T5E36. We took a particle count by using Nano Measure software to find out almost mono-dispersed T5E36 particles with diameters near

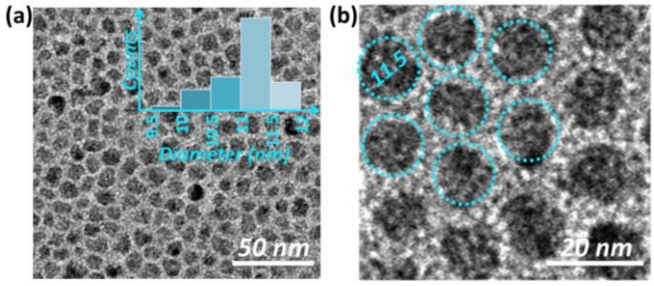

Fig. 8 a) TEM image with scale bar= 100 nm and particle count result of TEM image b) TEM image with scale bar= 20 nm

11.5 nm [38,39]. With the help of Scherrer equation [40],

$$D=K\gamma/(B\cos\vartheta)$$

where K is the Scherrer constant，γ is the X-ray wavelength, B is the peak width of the diffraction peak at half maximum height and ϑ is the diffraction angle. The correlation length D of column-column was calculated to be 11.3 nm from 1DXRD results which was fine consistent with the diameter of T5E36 particles in TEM images.

The intrinsic charge carrier mobility of T5E36 was

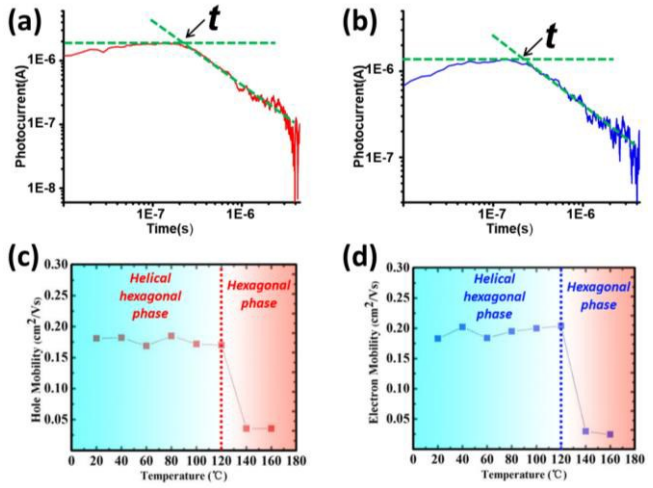

Fig. 9 Double logarithmic plots of typical transient current I as a function of time t of T5E36 in an electric field of E = 2.2 ×10^4 Vcm^{-1} at 20 °C: a) hole mobility of T5E36: μ_h = 1.76×10^{-1} $cm^2V^{-1}s^{-1}$; b) electron mobility of T5E36: μ_e = 1.77 ×10^{-1} $cm^2V^{-1}s^{-1}$; Mobility of T5E36 as a function of temperature from 20°C to 160 °C c) hole d) electron.

measured by time-of-flight (TOF) method from room temperature to 160°C [41]. At the isotropic temperature, the fully purified T5E36 was filled by capillary action into a liquid crystal cell consisted of two ITO glass substrates. A nitrogen pulse laser (λ =337nm, Pulse duration = 600 ps) irradiated the sample and generated charge carriers. The results of photocurrent were analyzed in double logarithmic plots recorded by a digital oscilloscope. The transient photocurrents for hole and electron of T5E36 at room temperature and mobility changes depending on temperatures were presented in Fig. 9. The non-dispersive curve with a plateau region followed by a sigmoidal decay indicated that the charge transport was Gaussian-type and can be described as a band-like transport model. The transit time t can be determined by the inflection point in the transient photocurrent curves and the charge carrier mobility can be calculated according to eqation below, where V and d were the applied voltage and sample thickness which was 9 μm here, respectively.

$$\mu=d^2/Vt$$

The hole and electron mobility can reach high up to 1.8×10^{-1} $cm^2V^{-1}s^{-1}$ and 2.0×10^{-1} $cm^2V^{-1}s^{-1}$ which were much higher than previously reported works while the mobility of most triphenylene derivatives without forming helical superlattice nanostructure was 10^{-2}~10^{-3} $cm^2V^{-1}s^{-1}$ [42,43]. As temperature raised higher than 120°C, the mobility of T5E36 exhibited a sudden decline which was entirely accorded with the transtion from helical hexagonal phase to hexagonal phase on heating. Thus,we can draw a conclusion that the formation of helical superlattice nanostructure notably improved bipolar charge carrier mobility.

Conclusions

In summary, we have successfully synthesized a series of triphenylene esters with ester groups at different substituent positions. After ample analyzation of the POM, DSC, 1DXRD, 2DXRD, EDM and ESP results, we demonstrate that only T5E36 with two ester groups out of plane in the contrary direction self-assembles to form a 9_1 right-handed helical ordered superlattice structure.The TEM images testify a mono-dispersion of T5E36 particles with diameter near 11.5 nm which approximately equal to the correlation length of column-column.Finally, intrinsic charge carrier mobility of T5E36 measured by TOF method manifests unprecedented high hole and electron mobility up to 10^{-1} $cm^2V^{-1}s^{-1}$ during its helical phase.These results are expected to play an important role in elucidations of fundamental aspects of self-assembly and applications on optoelectronic devices based on ester-modified triphenylene derivatives.

Conflicts of interest

There are no conflicts to declare

Acknowledgements

This work is supported by State Key Laboratory for Mechanical Behavior of Materials (20171913), the Natural Science Foundation of China (No. 51702019), the Beijing Natural Science Foundation of China (2172024), the Beijing Municipal Education Commission Project under Grant (No.

KM201210015008), the Beijing Municipal Commission of Education Foundation for Ability Construction of Scientific and Technological Innovation Service (Research on Nanoscale Copper Conductive Ink, PXM2017_014223_000036).

Notes and references

1 P. G. Schouten, J. M. Warman, M. P. de Haas, C. F. van Nostrum, G. H. Gelinck, R. J. M. Nolte, M. J. Copyn, J. W. Zwikker and M. K. Engel, *Journal of the American Chemical Society*, 1994, **116**, 6880-6894.
2 S. Sergeyev, W. Pisula and Y. H. Geerts, *Chemical Society Reviews*, 2007, **36**, 1902-1929.
3 L. Schmidt-Mende, A. Fechtenkötter, K. Müllen, E. Moons, R. H. Friend and J. D. MacKenzie, *Science*, 2001, **293**, 1119.
4 B. R. Kaafarani, *Chemistry of Materials*, 2011, **23**, 378-396.
5 A. M. van de Craats, N. Stutzmann, O. Bunk, M. M. Nielsen, M. Watson, K. Müllen, H. D. Chanzy, H. Sirringhaus and R. H. Friend, *Advanced Materials*, 2003, **15**, 495-499.
6 H. Fujikake, T. Murashige, M. Sugibayashi and K. Ohta, *Applied Physics Letters*, 2004, **85**, 3474-3476.
7 C. Destrade, M. C. Mondon and J. Malthete, *J. Phys. Colloques*, 1979, **40**, C3-17-C13-21.
8 A. BÉGuin, J. Billard, J. C. Dubois, N. H. Tinh and A. Zann, *J. Phys. Colloques*, 1979, **40**, C3-15-C13-16.
9 S. Chandrasekhar, B. K. Sadashiva and K. A. Suresh, *Pramana*, 1977, **9**, 471-480.
10 J. Billard and B. K. Sadashiva, *Pramana*, 1979, **13**, 309-318.
11 C. Destrade, N. H. Tinh, H. Gasparoux, J. Malthete and A. M. Levelut, *Molecular Crystals and Liquid Crystals*, 1981, **71**, 111-135.
12 A. M. Levelut, F. Hardouin, H. Gasparoux, C. Destrade and T. Nguyen Huu, *J. Phys. France*, 1981, **42**, 147-152.
13 M. Manickam and S. Kumar, *Molecular Crystals and Liquid Crystals*, 1999, **326**, 165-176.
14 S. Kumar, *Liquid Crystals*, 2004, **31**, 1037-1059.
15 I. G. Voigt-martin, R. W. Garbella and M. Schumacher, *Liquid Crystals*, 1994, **17**, 775-801.
16 S. U. Vallerien, M. Werth, F. Kremer and H. W. Spiess, *Liquid Crystals*, 1990, **8**, 889-893.
17 M. Werth, S. U. Vallerien and H. W. Spiess, *Liquid Crystals*, 1991, **10**, 759-770.
18 A. Kettner and J. H. Wendorff, *Liquid Crystals*, 1999, **26**, 483-487.
19 T. Osawa, T. Kajitani, D. Hashizume, H. Ohsumi, S. Sasaki, M. Takata, Y. Koizumi, A. Saeki, S. Seki, T. Fukushima and T. Aida, *Angewandte Chemie International Edition*, 2012, **51**, 7990-7993.
20 M.-C. Yeh, Y.-L. Su, M.-C. Tzeng, C. W. Ong, T. Kajitani, H. Enozawa, M. Takata, Y. Koizumi, A. Saeki, S. Seki and T. Fukushima, *Angewandte Chemie International Edition*, 2013, **52**, 1031-1034.
21 W. Zhang, S. Zhang, Z. Zhang, H. Yang, A. Zhang, X. Hao, J. Wang, C. Zhang and J. Pu, *The Journal of Physical Chemistry B*, 2017, **121**, 7519-7525.
22 Z. Zhang, H. Yang, J. Bi, A. Zhang, Y. Fang, Y. Feng, L. An, L. Liang, C. Zhang and J. Pu, *New Journal of Chemistry*, 2018, **42**, 20087-20094.
23 Z. Zhang, H. Yang, A. Zhang, J. Bi, Y. Feng, W. Zhang, C. Zhang and J. Pu, *Journal of Materials Chemistry C*, 2018, **6**, 5597-5600.
24 N. Boden, R. J. Bushby, A. N. Cammidge and P. S. Martin, *Journal of Materials Chemistry*, 1995, **5**, 1857-1860.
25 N. Boden, R. J. Bushby and A. N. Cammidge, *Journal of the American Chemical Society*, 1995, **117**, 924-927
26 H. Wu, C. Zhang, J. Pu and Y. Wang, *Liquid Crystals*, 2014, **41**, 1173-1178.
27 M. T. Allen, K. D. M. Harris, B. M. Kariuki, N. Kumari, J. A. Preece, S. Diele, D. Lose, T. Hegmann and C. Tschierske, *Liquid Crystals*, 2000, **27**, 689-692.
28 S. K. Prasad, D. S. S. Rao, S. Chandrasekhar and S. Kumar, *Molecular Crystals and Liquid Crystals*, 2003, **396**, 121-139.
29 Z. Chen, U. Baumeister, C. Tschierske and F. Würthner, *Chemistry – A European Journal*, 2007, **13**, 450-465.
30 S. Laschat, A. Baro, N. Steinke, F. Giesselmann, C. Hägele, G. Scalia, R. Judele, E. Kapatsina, S. Sauer, A. Schreivogel and M. Tosoni, *Angewandte Chemie International Edition*, 2007, **46**, 4832-4887.
31 C. Roche, H.-J. Sun, M. E. Prendergast, P. Leowanawat, B. E. Partridge, P. A. Heiney, F. Araoka, R. Graf, H. W. Spiess, X. Zeng, G. Ungar and V. Percec, *Journal of the American Chemical Society*, 2014, **136**, 7169-7185.
32 C. Roche, H.-J. Sun, P. Leowanawat, F. Araoka, B. E. Partridge, M. Peterca, D. A. Wilson, M. E. Prendergast, P. A. Heiney, R. Graf, H. W. Spiess, X. Zeng, G. Ungar and V. Percec, *Nature Chemistry*, 2015, **8**, 80.
33 M. Peterca, V. Percec, M. R. Imam, P. Leowanawat, K. Morimitsu and P. A. Heiney, *Journal of the American Chemical Society*, 2008, **130**, 14840-14852.
34 C. Knupp and J. M. Squire, *Journal of Applied Crystallography*, 2004, **37**, 832-835.
35 S.-X. Fa, X.-F. Chen, S. Yang, D.-X. Wang, L. Zhao, E.-Q. Chen and M.-X. Wang, *Chemical Communications*, 2015, **51**, 5112-5115.
36 V. Percec, H.-J. Sun, P. Leowanawat, M. Peterca, R. Graf, H. W. Spiess, X. Zeng, G. Ungar and P. A. Heiney, *Journal of the American Chemical Society*, 2013, **135**, 4129-4148.
37 M. J. Frisch, G. W. Trucks, H. B. Schlegel, G. E. Scuseria, M. A. Robb, J. R. Cheeseman, G. Scalmani, V. Barone, B. Mennucci, G. A. Petersson, Gaussian 09, Revision C.01; Gaussian, Inc., Wallingford, CT, 2011.
38 X.-Q. Wei, G. F. Payne, X.-W. Shi and Y. Du, *Soft Matter*, 2013, **9**, 2131-2135.
39 L. Zeng, Q.-H. Guo, Y. Feng, J.-F. Xu, Y. Wei, Z. Li, M.-X. Wang and X. Zhang, *Langmuir*, 2017, **33**, 5829-5834.
40 A. Monshi, M. R. Foroughi and M. Reza Monshi, *World Journal of Nano Science and Engineering*, 2012, **2**, 154-160.
41 V. Podzorov, E. Menard, A. Borissov, V. Kiryukhin, J. A. Rogers and M. E. Gershenson, *Physical Review Letters*, 2004, **93**, 086602.
42 M. Kumar and S. Kumar, *Polymer Journal*, 2016, **49**, 85
43 T. Wöhrle, I. Wurzbach, J. Kirres, A. Kostidou, N. Kapernaum, J. Litterscheidt, J. C. Haenle, P. Staffeld, A. Baro, F. Giesselmann and S. Laschat, *Chemical Reviews*, 2016, **116**, 1139-1241.

View Article Online
DOI: 10.1039/C9TC04349G